Letters in Applied NanoBioScience
Open-Access Journal (ISSN: 2284-6808)

Article
Volume 15, Issue 1, 2026, 22
https://doi.org/10.33263/LIANBS151.022

Phytomediated Synthesis of Flower-Plated Reduced Graphene Oxide Nanosheets for Breast Cancer Therapy: Cytotoxicity and Genotoxicity in MCF-7 Cells

Amenah Salim Kadhim [1], Zainab Shakir Abdullah Al-Ali [2,*]

[1] Department of Chemistry, College of Science, Thi-Qar University, Thi-Qar 64001, Iraq
[2] Department of Chemistry, College of Science, Basrah University, Basrah 61004, Iraq
* Correspondence: zainab.abdulah@uobasrah.edu.iq;

Received: 18.08.2025; Accepted: 20.02.2026; Published: 30.03.2026

Abstract: This study reports a green, one-step synthesis of reduced graphene oxide (MERCL-rGO) using a methanolic extract of *Rhus coriaria* (L.) leaves (MERCL) as a reducing agent. The successful bioreduction was confirmed by comprehensive characterization. UV-Vis spectroscopy showed a redshifted absorption peak at 250 nm, while Raman spectra indicated an increased I_D/I_G ratio (1.08), confirming defect generation. XRD and TEM analyses revealed a crystalline, flower plate nanostructure with an average size of 9.6 nm. The cytotoxicity of the synthesized MERCL-rGO nanosheets was evaluated in MCF-7 breast cancer cells, with a dose-dependent reduction in cell viability and an IC50 of 212.84 µg/ml. Furthermore, the alkaline comet assay demonstrated significant genotoxicity at the IC50 concentration, inducing DNA damage in treated cells. The findings suggest that the phytochemicals in the leaf have promising potential as cytotoxic and genotoxic agents against breast cancer cells, warranting further investigation for therapeutic applications.

Keywords: bioreduction; *Rhus coriaria* (L.); reduced graphene oxide; anticancer activity.

1. Introduction

Cancer remains a leading cause of mortality worldwide, with breast cancer being one of the most prevalent and challenging malignancies to treat [1-3]. Breast cancer is a heterogeneous disease and occurs due to several factors such as smoking, obesity, alcohol consumption, family history, and age [4-6]. Conventional therapies like chemotherapy, while effective, often cause severe side effects and face limitations due to drug resistance [7-9]. This has spurred the search for novel, more selective therapeutic agents. In this context, nanotechnology offers promising platforms, with graphene-based nanomaterials emerging as potent tools for cancer therapy, biosensors, drug delivery, and bioimaging [10-14]. Among them, reduced graphene oxide (rGO) is particularly attractive due to its high surface area, unique electrical properties, and potential for functionalization [15]. rGO is used in various cancer treatments, including chemotherapy and photothermal therapy [16,17]. However, conventional chemical methods for rGO synthesis often involve toxic reducing agents [18]. Consequently, green synthesis using plant extracts as reducing and stabilizing agents has gained significant interest as a safe, eco-friendly, and cost-effective alternative [19]. Previous

studies have successfully employed various plant extracts for the bioreduction of graphene oxide (GO), such as sugarcane bagasse, Kigelia Africana, Verbena officinalis, and Shallots [20-23]. *Rhus coriaria* (L.) (sumac) is a plant known for its high concentration of bioactive phytochemicals. While previous work has utilized fruit extract for rGO synthesis [24]. The leaf extract presents a distinct and largely unexplored phytochemical profile. Crucially, the methanolic extract of *Rhus coriaria* (L.) leaves (MERCL) is exceptionally rich in essential oils and their derivatives, such as oleic acid, in addition to triterpenoids and polyphenols, unlike the methanolic extract of *Rhus coriaria* (L.) fruits, which has a high percentage of essential oils, esters, and polyphenols [25]. The essential oils have proven effective as reducing agents in green nanosynthesis (nanoparticle synthesis), not just as polyphenols. Furthermore, studies have investigated the toxicity of nanosynthesis in cancer treatment, but polyphenols consistently highlight their role as reducing agents, particularly in nanomaterials [26–28]. Essential oils and their derivatives can act as effective reducing agents via their nucleophilic functional groups such as (-OH, -COOH), potentially facilitating GO reduction through mechanisms distinct from the purely polyphenol-driven pathways reported for other extracts [29,30]. Therefore, a research gap exists in understanding the efficacy and mechanism of GO reduction using an essential oil-dominated extract like MERCL, and in evaluating the biological activity of the resulting nanomaterial. This study aims to fill this gap by investigating the leaf extract of Iraqi *Rhus coriaria* (L.) as a novel bioreductant for the synthesis of rGO nanosheets (MERCL-rGO). We hypothesize that the unique phytochemical composition of MERCL will not only efficiently reduce GO but also yield rGO nanosheets with a distinct morphology and enhanced bioactivity. The synthesized MERCL-rGO was thoroughly characterized and its cytotoxicity and genotoxicity against MCF-7 breast cancer cells were evaluated to assess its potential for breast cancer therapy.

2. Materials and Methods

2.1. Materials.

Graphite powder (99.9%), sulpheric acid (H_2SO_4, 98%), phosphoric acid (H_3PO_4, 85%), potassium permanganate ($KMnO_4$, ≥99%), hydrogen peroxide (H_2O_2, 30%), hydrochloric acid (HCl, 37%), and ethanol (C_2H_5OH, 98%) were used for graphene oxide (GO) synthesis. Methanol (CH_3OH, 98%) was used for plant extraction. For cell culture and bioassays, RPMI-1640 medium, Fetal Bovine Serum (FBS), Trypsin-EDTA, MTT (3-(4,5-dimethylthiazol-2-yl)-2,5-diphenyltetrazolium bromide), and Dimethyl Sulfoxide (DMSO) were procured. The human breast cancer cell line (MCF-7) was obtained from the Iranian Biological Resource Center.

2.2. Methods.

2.2.1. *Rhus coriaria* (L.) plant leaves.

Fresh Iraqi *Rhus coriaria* (L.) leaves were gathered from Chamchamal city in Sulaymaniyah governorate of Iraq in August 2021, and categorized at the Department of Biology, Faculty of Science, University of Thi-Qar, Iraq, on the basis of a literature review [31]. The leaves were separated from other plant remains, rinsed twice with water to remove dust, and then rinsed again with deionized water to ensure no contaminants remained. Keep the

leaves at room temperature and away from light once they have dried for three days. Dried leaves were processed into a fine powder using a blender and kept at 4°C until required.

2.2.2. Iraqi *Rhus coriaria* (L.) leaves extract preparation.

A modified method [32] was used to create *Rhus coriaria* (L.) leaves methanolic extract (MERCL-rGO). Using a Buncher funnel to separate the extract from the solid material, 10 g of leaf powder was combined with 100 mL 70% methanol and agitated at 40°C for 30 minutes. The filter was mixed and dried at 40°C using a rotary evaporator. The material residue or dry powder is kept while being used.

2.2.3. Graphene oxide (GO) preparation.

By using the improved Hummer process [33], graphene oxide is produced. Using a stirrer, combine 40 mL of H_3PO_4 (15.18 M) with 360 mL of H_2SO_4 (18.4 M) in a 1:9 ratio. Add 3 g of graphite powder to the mixture, then gradually stir in 18 g of KMnO4 until the liquid turns dark green. The reaction mixture was placed in an ice bath with salt and agitated for 12 hours, with the temperature monitored with a thermometer to maintain 50°C. The reaction was poured into 400 mL of ice and 3 mL of 30% H_2O_2 after cooling to room temperature, yielding a yellow-colored solution. Following that, it was sieved and put through a polyester fabric filter. The liquid is poured into a sieve, filtered through the sieve, and then passed through a polyester cloth placed on top of the sieve. The precipitating material was then rinsed twice in 200 mL each of water, 30% HCl, and ethanol. Next, the filtrate was centrifuged (4000 rpm for 4 hours) while the supernatant was decanted away. The substance was gathered, coagulated with 200 mL of ether, and filtered through (Whatman no.1) filter paper. The finished product was vacuum-dried for an entire night at room temperature.

2.2.4. Bioreduction of reduced graphene oxide (MERCL-rGO).

Reduced graphene oxide was created from the methanolic extract of *Rhus coriaria* (L.) leaves (MERCL-rGO) [34], 100 mL of distilled water with 0.04 g of graphene oxide dissolved in it, to create the yellowish-brown reaction mixture.

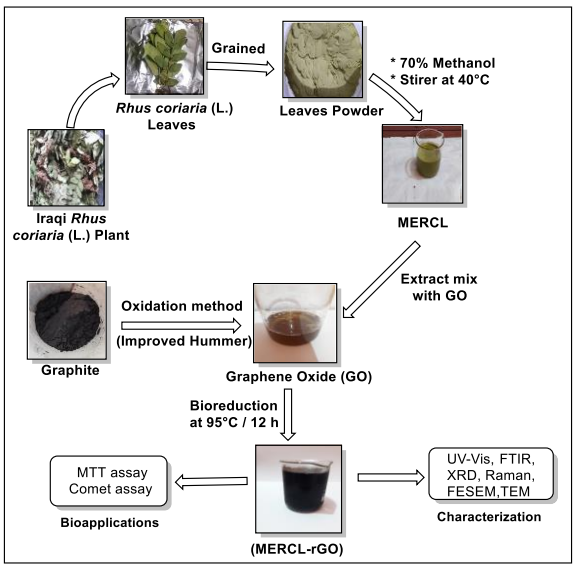

Figure 1. Schematic illustration of the green synthesis of MERCL-rGO by using the methanolic extract of Iraqi *Rhus coriaria* (L.) (MERC) and its subsequent biological evaluation against MCF-7 breast cancer cells. Where MERCL-rGO (Methanolic extract of Iraqi *Rhus coriaria* (L.)- reduced graphene oxide).

Mix 0.01 g of each dried extract of *Rhus coriaria* (L.) leaves with the GO solution. For 40 minutes, the reaction mixture is sonicated. The combination was reacted in a water bath at 95°C for 12 hours. GO's yellowish-brown color changed to black, demonstrating the effective removal of oxygen groups from GO. In order to achieve excellent, dried MERCL-rGO, the black color mixture was centrifuged at 10000 rpm for 10 minutes. The precipitated product was then rinsed with deionized water and vacuumed. The biosynthesized MERCL-rGO was stored in a vial for future characterization and biomedical application research. A schematic of the overall synthesis and testing workflow is presented in Figure 1.

2.2.5. Characterization.

The samples of graphene oxide (GO) and biosynthesized (MERCL-rGO) were characterized using several instruments. UV-Vis spectroscopy was identified on a UV-1900 device (Shimadzu, Japan). Fourier transform infrared (FTIR) spectroscopy was performed over a wavenumber range of (4000-400) cm^{-1} using an IRAffinity-1800 spectrometer (Shimizu, Japan). X-ray diffraction (XRD) analysis was conducted using a PW173 diffractometer (PHILIPS, Holland). Raman spectroscopy was carried out on a TahranN1-541 device (TESCAN, Iran). Surface morphology was examined via field emission scanning electron microscopy (FESEM) using a MIRA III microscope (TESCAN, Czech), while transmission electron microscopy (TEM) was performed using a Libra 120 instrument (CarZeiss, Germany). Finally, gas chromatography-mass spectrometry (GC/MS) analysis was conducted on an Agilent 7820A system (USA).

2.2.6. MTT assay.

With few modifications, the MTT assay [35] was used to assess the MERCL-rGO cytotoxicity. The cell line (MCF-7) was grown at a density of $1x10^5$ cells/well on a 96-well plate for 24 hours under ideal conditions (37°C, 5% CO_2 in a humidified incubator). After removing the growth medium (10% FBS), the cells were given two washes in phosphate buffer saline (PBS). The cells were then cultured for 72 hours in fresh maintenance RPMI media (10% FBS) with (12.5, 25, 50, 100, and 200 µg/mL) of MERCL-rGO. Each concentration was tested in three independent wells (n=3) to ensure reproducibility, with column elution buffer serving as the control. Each well received a 10 µL addition of freshly made 5 mg/mL MTT in PBS, which was then incubated for 4 hours. The media was taken out, and 100 µL/well of DMSO was added. To make the formazan crystals more soluble, plates were gently shaken (formazan dyes are purple, crystalline compounds generated by the reduction of tetrazolium salts via mitochondrial enzymes in viable cells). A microplate reader was used to measure the absorbance at 545 nm. The optical absorbance of the treatment groups was expressed as a percentage of the control group's mean absorbance, which was set to 100%. Half-maximal inhibitory concentration (IC_{50}) and the percentage of cell toxicity were estimated.

2.2.7. DNA fragmentation protocol.

The alkaline comet assay [36], with some modification, was used to measure DNA damage. In 25 cm^2 flasks, the MCF-7 cell line was grown for 24 hours at 37°C with 5% CO_2. They were then given MERCL-rGO treatment for 48 hours at IC_{50} concentration (37°C, 5% CO_2). Trypsinization, centrifugation, and two rinses in Mg- and Ca-free, ice-cold PBS were performed on the cells before they were centrifuged (1000 rpm, 5 minutes) in fresh culture

media. Low-melting-point agarose (Type VII) was used to treat the cells ($1x10^4$) before they were transferred to a glass slide that had already been covered with high-melting-point agarose (Type I). The slides were then submerged for 60 minutes at 4°C in a lysis solution made up of 2.5 M NaCl, 100 mM EDTA, 10 mM Tris, and 1% Triton X-100. After cell lysis in the solidified agarose, DNA was unraveled by an alkaline process. After the cells were lysed in the agarose that had solidified, DNA was unraveled using an alkaline solution. The slides were then washed for 30 minutes at 4°C in electrophoresis buffer (TBE) (300 mM NaOH and 1 mM EDTA, pH > 13). Then, electrophoresis was performed for 20 minutes at 4°C with a voltage of 1.0 V/cm and a 490 mA intensity. It was stained using the EtBr (0.5 g/mL) technique. In this test, DNA migration distance gauges the degree of DNA damage under a certain circumstance. Comet slides were electrophoretically separated and then fixed in 100% alcohol for 10 minutes after being rinsed in 0.4 M Tris-HCl (pH 7.5). Each slide was counted for 100 nuclei, and the percentage of cells with and without DNA damage was calculated. The cells were separated into two groups for the count: those with undamaged DNA and those with damaged DNA. The DNA damage was documented using a fluorescence microscope. It is split into the following five classes based on tail size: Class 1 has no tail, Class 2 has a tail that is shorter than the diameter of the head (nucleus), Class 3 has a tail that is 1-2 times the diameter of the head, and Class 4 has a tail that is longer.

3. Results and Discussion

3.1. UV-Vis spectroscopy of MERCL-rGO.

The successful bioreduction of GO to MERCL-rGO using the methanolic extract of Iraqi Rhus coriaria (L.) leaves (MERCL) was confirmed through a series of spectroscopic analyses. The UV-Vis absorption spectrum of graphite, GO, and MERCL-rGO is displayed in Figure 2. It shows an absorbance peak at 282 nm for the graphite sample, which represents the electronic transition (π-π*) of the aromatic C=C bonds [37]. Following oxidation, the UV-Vis spectra of GO showed an absorption peak at 226 nm, corresponding to (π-π*) transition of the aromatic C=C bonds, and a shoulder at 296 nm attributed to the (n-π*) transitions of aromatic C=O bonds [38]. After bioreduction, the spectrum of MERCL-rGO exhibited a notable red shift of this peak to 250 nm. This shift is a classic indicator of the restoration of the conjugated carbon network within graphene, which aligns with reports for plant-based rGO synthesis, such as the shift from 230 nm to 270 nm observed using Clinacanthus nutans [39] and Ocimum sanctum L. [40]. This shift confirmed the bioreduction of GO to MERCL-rGO successfully.

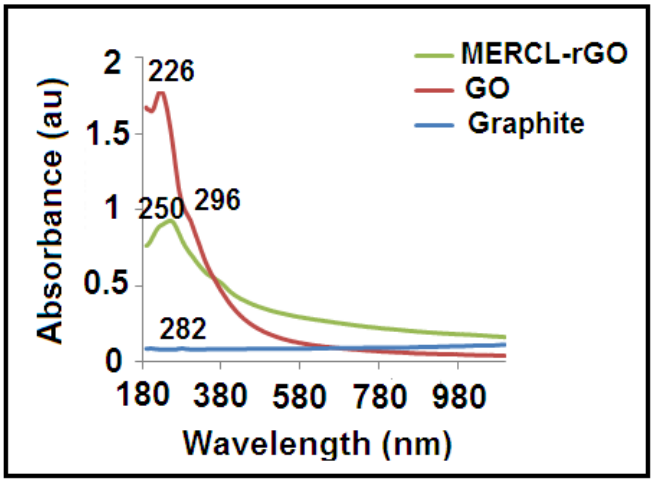

Figure 2. UV-Vis spectrum of MERCL-rGO, GO, and graphite.

3.2. FTIR spectra of MERCL-rGO.

The results of the FTIR measurements performed on the three samples. The carbon structure of graphite was revealed in the FTIR spectra by a low-intensity peak at 1639 cm-1, which indicated the stretching vibration of the (C=C) bond. The FTIR spectrum of GO displayed prominent bands at (3360 cm^{-1} -1454 cm^{-1}), representing the stretching vibration and bending vibration of the hydroxyl group (-OH), respectively [41,42]. Additionally, the spectra appeared peaks at (2920 cm^{-1}-2850 cm^{-1}), 1739 cm^{-1}1620 cm^{-1}, 1222 cm^{-1}, and 1053 cm^{-1}, which are attributed to -CH bond stretching vibration, the carbonyl group (C=O), stretching of the C=C bond, the C-O of the alkoxy and epoxy bonds, respectively [43,44], in the MERCL-rGO spectrum. The peaks at 3387 cm^{-1} and 1381 cm^{-1} indicated the stretching and bending vibrations of the (-OH) group, respectively. The persistence of a broad (–OH) band can be attributed to the phytomolecules from the MERCL extract adsorbed on the rGO surface, which also contribute to its stabilization. In this spectrum, the intensity of the C=O band at 1739 cm^{-1} disappeared significantly, indicating the removal of oxygen-containing functional groups [45]. The decrease in intensity of the carbonyl band is more pronounced than in rGO synthesised using Citrullus colocynthis [46]. Additionally, the stretching vibration of the C=C band was indicated by the peak at 1612 cm^{-1}. The peaks at 1234 cm^{-1} and 1099 cm^{-1} were attributed to the vibration of the epoxy and alkoxy groups, respectively [47]. Suggesting a high reduction efficiency for MERCL, as shown in Figure 3.

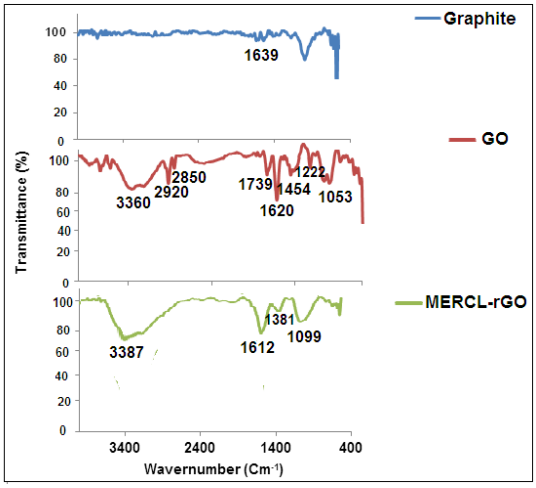

Figure 3. FTIR spectroscopy of Graphite, GO, and MERCL-rGO.

3.3. XRD of MERCL-rGO.

The XRD spectrum was used to investigate the crystalline structure and interlayer spacing (d-spacing). As presented in Figure 4, graphite showed a sharp peak at 26.68° (d-spacing = 0.334 nm) [48]. Upon oxidation, this peak shifted to 11.42° in the GO spectra, corresponding to an increased d-spacing of 0.789 nm due to the intercalation of water molecules and the formation of oxygen groups between the layers of graphite [49,50]. After bioreduction, the MERCL-rGO pattern displayed a number of peaks and a broad peak at 27.21°, indicating a restored graphitic structure with a reduced d-spacing of 0.3276 nm [51]. The d-spacing of MERCL-rGO is closer to graphite than to GO, confirming the effective removal of intercalated oxygen moieties. This value is comparable to, or slightly lower than, other bio-reduced rGO reports, such as rGO from *Zanthoxylum acanthopodium* (d-space = 0.36 nm) [52]. Suggesting efficient layer stacking in our synthesized material. The crystal size (D) of graphite, GO, and MERCL-rGO was calculated by Scherrer's equation as shown in eq. (1), 28.90 nm,

10.42 nm, and 40.37 nm, respectively. Further categorization within the results can be achieved using subsections where necessary.

$$D = \frac{K\lambda}{\beta \cos\theta} \quad (1)$$

Where D= Crystal size, nm; K = Constant equal, 0.9; λ= wavelength, 0.154 nm; β= FWHM (Full width at half maximum intensity), radians; θ= Bragg angle.

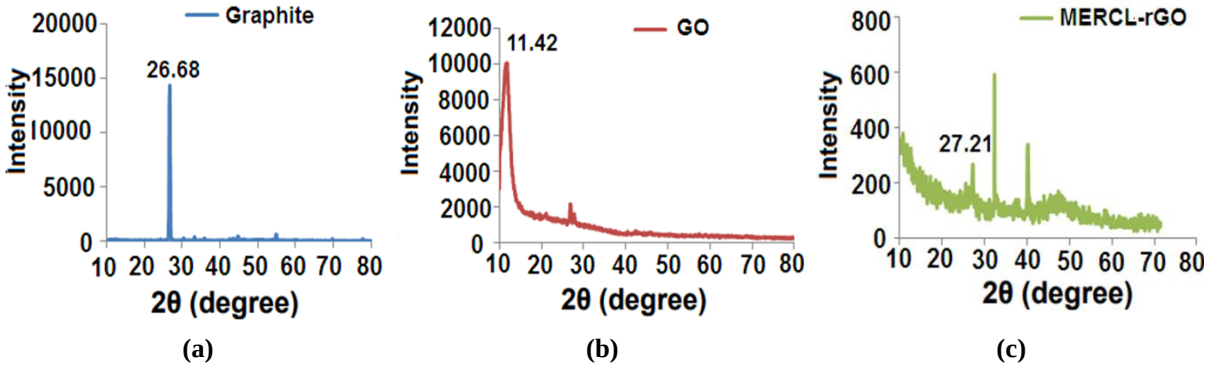

(a) **(b)** **(c)**

Figure 4. XRD spectra of (**a**) graphite; (**b**) GO; (**c**) MERCL-rGO.

3.4. Raman spectroscopy of MERCL-rGO.

To analyze the significant structural variations caused by the chemical transformations of graphite, GO, and MERCL-rGO, these transformations were identified using Raman spectroscopy. Figure 5 shows Raman spectra of three samples: graphite, GO, and MERCL-rGO. The Raman spectrum of graphite pattern showed three bands: the D-band at1330 cm^{-1} (associated with structural defects or loss of translation symmetry (A_{1g}) and disordered sp^3 carbon), the G-band at 1576 cm^{-1} (related to the in-plane vibration of sp^2-hybridized carbon and reflected the first-order scattering of the E_{2g} mode), and 2D at 2688 cm^{-1} (refered to the rearrangement of the graphite's structural framework along the axis), respectively [53]. After oxidation, the Raman spectrum of GO showed the D-band and G band at 1353 cm^{-1} and 1597 cm^{-1}, respectively. In contrast to these, the MERCL-rGO Raman spectra showed the D and G bands at 1330 cm^{-1} and 1590 cm^{-1}, respectively [54]. The intensity ratio of these bands (I_D/I_G) is a key metric for defect density; the intensity ratio (I_D/I_G) increased from 0.84 for GO to 1.08 for MERCL-rGO. This increase in the (I_D/I_G) ratio is a direct consequence of the reduction process. While the creation of new, smaller graphitic domains during the removal of oxygen functional groups introduces more defects and edges, it also restores sp^2 clusters. The net effect is often an increase in overall defect density relative to the pre-reduction GO, consistent with successful bioreduction reported in other studies [55]. This higher defect density in MERCL-rGO could provide more active sites for biomolecular interactions, potentially influencing its biological activity.

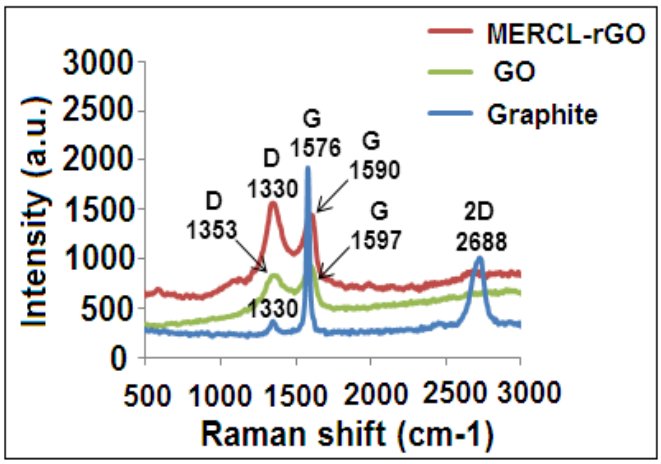

Figure 5. Raman spectra of graphite, GO, and MERCL-rGO.

3.5. FESEM of MERCL-rGO.

The surface morphology of GO and MERCL-rGO was examined using FESEM. The FESEM image of GO shows Figure 6a, which revealed a characteristic wrinkled, sheet-like morphology with a smooth, way surface because the intercalation of the oxygen functional groups (epoxy, carboxylic, and hydroxyl) on the surface GO by oxidation resulted in the sheets becoming more free to move when the measurement was zoomed in to a small nanoscale that revealed the thickness at the range of (14.11-30.59 nm) [56]. In contrast, the MERCL-rGO image (Figure 6b) shows a unique, distinct flower-plate nanostructure, with petals ranging in size from 15.3 to 62.6 nm. This novel morphology suggests that the phytochemicals in MERL not only reduce GO but also direct its assembly into a specific architecture during the synthesis process [57].

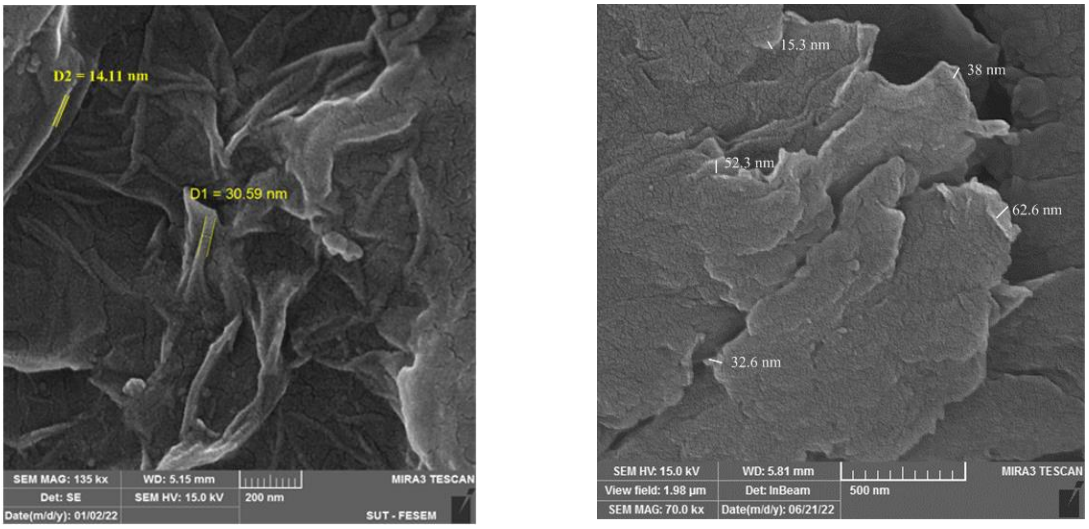

(a) **(b)**

Figure 6. FESEM images of (**a**) GO; (**b**) MERCL-rGO.

3.6. TEM of MERCL-rGO.

TEM analysis provided further insight into the nanostructure. TEM image of GO (Figure 7a) appeared as thin sheets, transparent, and folded layers with a measured thickness of approximately 15.54 nm [58]. TEM image of MERCL-rGO (Figure 7b) revealed a layer with a maximum thickness of 9.2 nm. This supports the idea that rGO forms from a thin layer. It was found that MERCL-rGO has a lower thickness and fewer folds than GO and MERCL-

rGO, typical of a single graphene sheet that has been thoroughly exfoliated [59], and is superior for biological applications.

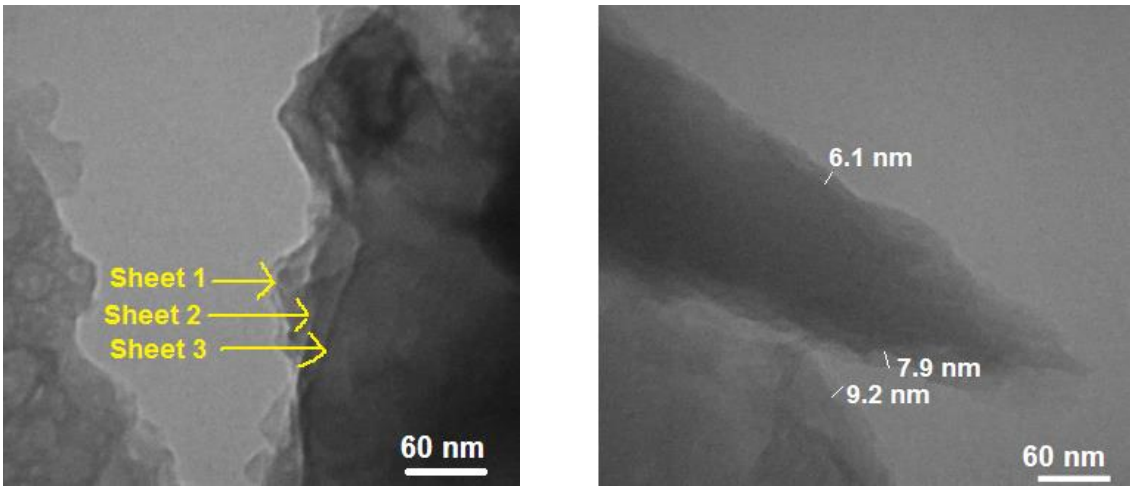

(a) **(b)**

Figure 7. TEM images of (**a**) GO; (**b**) MERCL-rGO.

3.7. Iraqi Rhus coriaria (L.) leaves methanolic extract GC/MS analysis.

The resultant extract was analyzed using GC/MS. The GC/MS spectrum of the methanolic extract (MERCL) Figure 8 revealed 30 phytochemical compounds, which summarized in a streamlined Table 1 focusing on the major constituents of essential oils (44.32%), Table 2 represented compounds of essential oils esters (28.18%), Table 3 included compounds of triterpenoids (14.89%), Table 4 explained constituents of phytosterols (4.87%), Table 5 showed compounds of alcohols (4.02%), other significant classes included polyphenols (1.13%), aldehydes (1.04%), cyclic amide (0,88%), and peroxides (0.68%), in Table 6, Table 7, and Table 8, respectively, which represent the constituets of the major phytochemicals in the methanolic extract (MERCL). Further categorization within the results can be achieved using subsections where necessary.

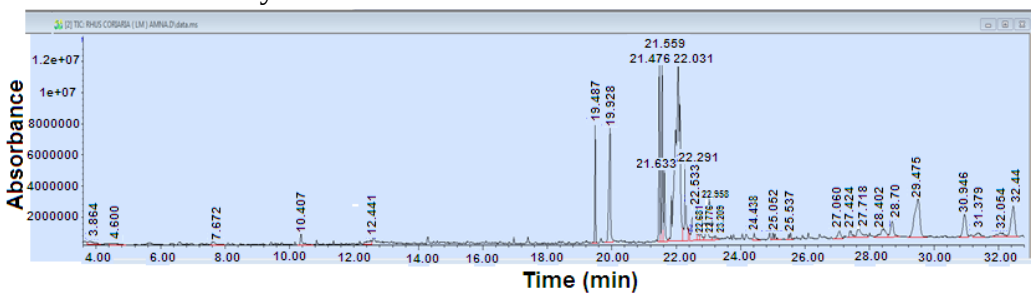

Figure 8. GC/MS chromatogram of a methanolic extract of *Rhus coriaria* (L.) leaves.

Table 1. The phytochemical compounds of essential oils (44.32%) in MERCL were identified by GC/MS.

NO.	Reaction time (min)	Area (%)	Compound identified	Molecular formula	Molecular weight (g/mol)	Structural
1	22.031	31.76	Oleic acid	$C_{18}H_{34}O_2$	282.5	
2	19.928	7.08	n-Hexadecanoic acid	$C_{16}H_{32}O_2$	256.43	
3	22.291	4.46	Octadecanoic acid	$C_{18}H_{36}O_2$	284.5	
4	22.776	0.58	9,12-octadecadienoic acid (Z,Z)	$C_{18}H_{32}O_2$	280.46	
5	24.438	0.44	9-Octadecenoic acid (E)	$C_{18}H_{34}O_2$	282.46	

Table 2. The phytochemical compounds of essential oils esters (28.18%) in MERCL were identified by GC/MS.

NO.	Reaction time (min)	Area (%)	Compound identified	Molecular formula	Molecular weight (g/mol)	Structural
1	21.559	7.40	9-Octadecanoic acid, methyl ester(E)	$C_{19}H_{36}O_2$	296.48	
2	21.476	6.38	9,12-Octadecadienoic acid (Z,Z)-, methyl ester	$C_{19}H_{34}O_2$	294.47	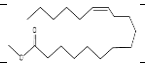
3	19.487	3.79	Hexadecanoic acid, methyl ester	$C_{17}H_{34}O_2$	270.45	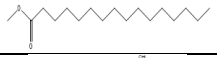
4	22.533	3.67	9,12-Octadecadienoic acid, methyl ester	$C_{19}H_{34}O_2$	294.47	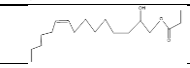
5	21.633	3.17	11-Octadecenoic acid, methyl ester	$C_{19}H_{36}O_2$	296.49	
6	22.958	2.02	2-Chloroethyl linoleate	$C_{20}H_{35}Cl_2O$	342.9	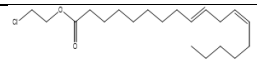
7	27.424	0.72	9-Octadecenoic acid (Z),2-hydroxy-1-(hydroxymethyl) ethyl ester	$C_{21}H_{40}O_4$	356.5	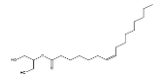
8	4.600	0.51	Acetic acid, hydroxy, ethyl ester	$C_4H_8O_3$	104.10	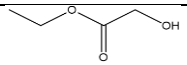

Table 3. The phytochemical compounds of triterpenoids (14.89%) in MERCL were identified by GC/MS.

NO.	Reaction time (min)	Area (%)	Compound identified	Molecular formula	Molecular weight (g/mol)	Structural
1	29.475	7.68	2,2,4a,6a,9,12b,14a-Octamethyl-1,2,3,4,4a,5,6,6a,6b,7,8,8a,9,12,12a 12b,13,14,14a,14b-eicosahydropicene	$C_{30}H_{50}$	410	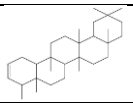
2	32.44	4.41	β Amyrin	$C_{30}H_{50}O$	426.7	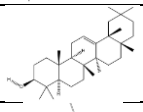
3	30.946	2.80	Lupeol	$C_{30}H_{50}O$	426.7	

Table 4. The phytochemical compounds of phytosterols (4.87%) in MERCL were identified by GC/MS.

NO.	Reaction time (min)	Area (%)	Compound identified	Molecular formula	Molecular weight (g/mol)	Structural
1	28.70	1.93	β-Sitosterol	$C_{29}H_{50}O$	414.7	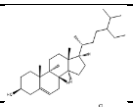
2	32.054	1.09	C(14a)-Homo-27-nor-14.beta.-gammaceran-3.alpha.-ol	$C_{28}H_{48}O_4$	428.7	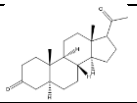
3	31.379	0.99	3,20-Allopregnanedione	$C_{21}H_{32}O_2$	316.48	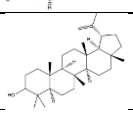
4	27.060	0.86	Stigmasterol	$C_{29}H_{48}O$	421.702	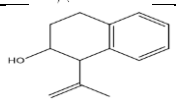

Table 5. The phytochemical compounds of alcohols (4.02%) in MERCL were identified by GC/MS.

NO.	Reaction time (min)	Area (%)	Compound identified	Molecular formula	Molecular weight (g/mol)	Structural
1	27.718	1.78	2-methyl-Z,Z-3,13-octadecadienol	$C_{19}H_{36}O$	280.5	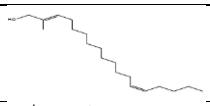
2	28.402	1.73	Cedran-diol, (8S,14)	$C_{15}H_{26}O_2$	238.36	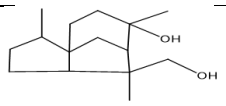

3	25.537	0.53	1-(2-methyl-allyl)-1,2,3,4-tetrahydronaphythyalen-2-ol	$C_{14}H_{18}O$	202.29	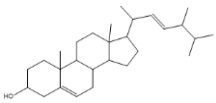

Table 6. The phytochemical compounds of polyphenols (1.13%) in MERCL were identified by GC/MS.

NO.	Reaction time (min)	Area (%)	Compound identified	Molecular formula	Molecular weight (g/mol)	Structural
1	7.672	0.43	Gallic acid	$C_7H_6O_5$	170.12	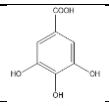
2	12.441	0.7	1,2,3-Benzenentriol	$C_6H_6O_3$	126.11	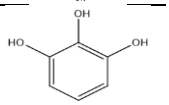

Table 7. The phytochemical compounds of aldehydes (1.04%) in MERCL were identified by GC/MS.

NO.	Reaction time (min)	Area (%)	Compound identified	Molecular formula	Molecular weight (g/mol)	Structural
1	25.052	0.56	9-Octadecenal (Z)	$C_{18}H_{34}O$	266.5	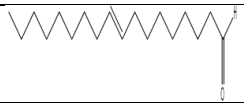
2	23.209	0.48	Cyclopropaneoctanal-2-octyl	$C_{19}H_{36}O$	280.5	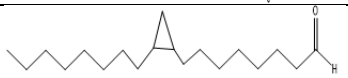

Table 8. The phytochemical compounds of cyclic amide (0.88%) and peroxide (0.68%) in MERCL were identified by GC/MS.

NO.	Reaction time (min)	Area (%)	Compound identified	Molecular formula	Molecular weight (g/mol)	Structural
1	10.407	0.88	Caprolactam	$C_6H_{11}NO$	113.16	
2	3.864	0.68	Hydroperoxide, pentyl	$C_5H_{12}O_2$	104.15	

The presence of these bioactive compounds, particularly those bearing active functional groups (-OH, -COOH), is crucial for reducing and stabilizing GO. Oleic acid, along with polyphenols such as gallic acid, likely acts as the primary reducing agent, facilitating the conversion of GO to rGO via nucleophilic reactions with epoxy and carbonyl groups, as illustrated in the proposed mechanism (Figure 9).

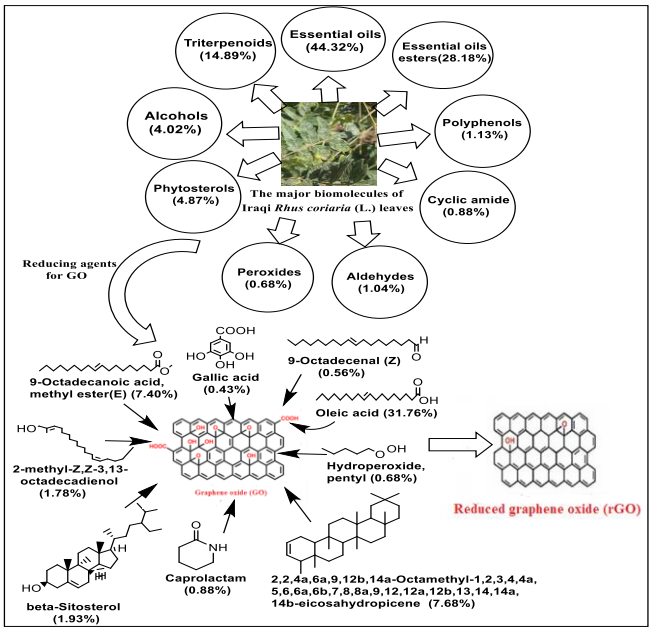

Figure 9. Mechanism proposed for the production of rGO using the key constituents of the leaves of Iraqi *Rhus coriaria* (L.).

3.8. Cytotoxicity of MERCL-rGO.

The anticancer potential of MERCL-rGO was evaluated against MCF-7 breast cancer cells. The MTT assay revealed a dose-dependent decrease in cell viability upon treatment with MERCL-rGO for 72 hours, shown in Figure 10. The cell viability dropped from 91.94% at 12.5µg/mL to 56.05% at 200 µg/mL. The half-maximal inhibitory concentration (IC_{50}) was calculated to be 212.8 µg/ml. Nevertheless, this dose-dependent trend is clear and aligns with the known cytotoxicity of the graphene family, which can induce cell death by compromising membrane integrity, inhibiting cell adhesion, and inducing oxidative stress [60,61]. The observed activity can also be synergistically enhanced by the bioactive phytochemicals from MERCL, such as triterpenoids and polyphenols, which are known for their anticancer properties [62,63].

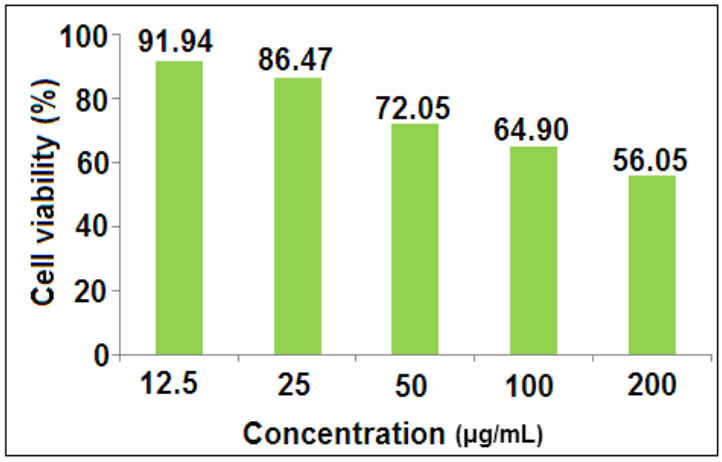

Figure 10. MERCL-rGO's ability to prevent the spread of MCF-7.

3.10. Genotoxicity of MERCL-rGO.

To investigate the mechanism of cell death, the genotoxic effect of MERCL-rGO was assessed using the alkaline comet assay. The comparison between (a) untreated control cells, which exhibit intact nuclei with no DNA migration, and (b) cells treated with MERCL-rGO at the IC_{50} concentration is represented in Figure 11. The treated cells displayed clear comet formations with elongated tails, indicative of significant DNA strand breaks. This genotoxicity is likely indirect, mediated by the generation of reactive oxygen species (ROS) upon MERCL-rGO's cellular internalization. ROS can cause oxidative damage to DNA, leading to single- and double-strand breaks that ultimately trigger apoptosis or other cell death pathways [64]. The finding that MERCL-rGO causes DNA damage provides a crucial mechanistic insight into its cytotoxic action and underscores its potential as a genotoxic agent for cancer therapy. This work reveals genotoxic effects of MERCL-rGO via the comet assay, linking DNA damage to phytochemical-driven ROS generation. Notably, the IC_{50} (212.84 µg/ml) is lower than chemically synthesized rGO (e.g., 350 µg/mL), Krętowski and Cechowska-Pasko [65], suggesting synergy between rGO's physical properties and MERCL's bioactive compounds. The proposed mechanism of rGO's effect on cancer cells, as shown in Figure 12, is that rGO attacks and penetrates the cell membrane, generating ROS that are key to DNA damage, mitochondrial dysfunction, protein damage, and ultimately cell death. The ultra-thin layered morphology (FESEM/TEM) and retained oxygen groups (FTIR) of MERCL-rGO facilitate membrane interaction and drug-loading potential. This contrasts with aggregates formed by chemical reduction Gul *et al.* [66], highlighting MERCL's role in stabilizing nanostructures.

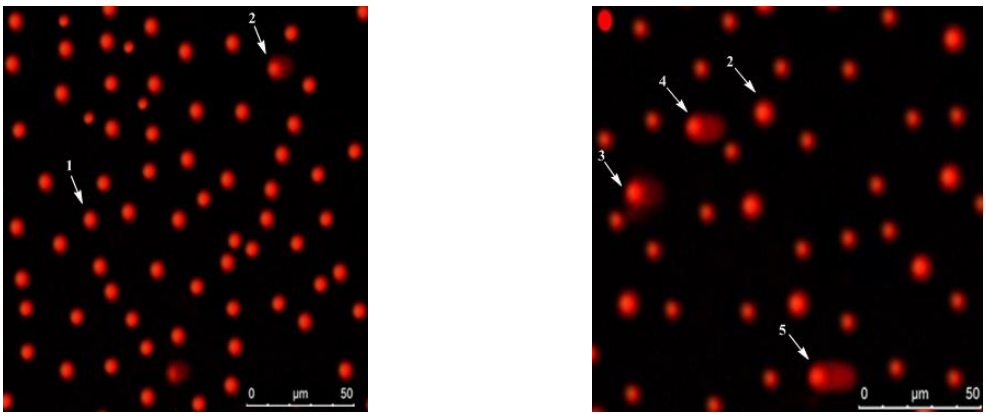

(a) **(b)**

Figure 11. Comet assay of MERCL-rGO effect on MCF-7 cells: **(a)** untreated (control); **(b)** treated with MERCL-rGO.

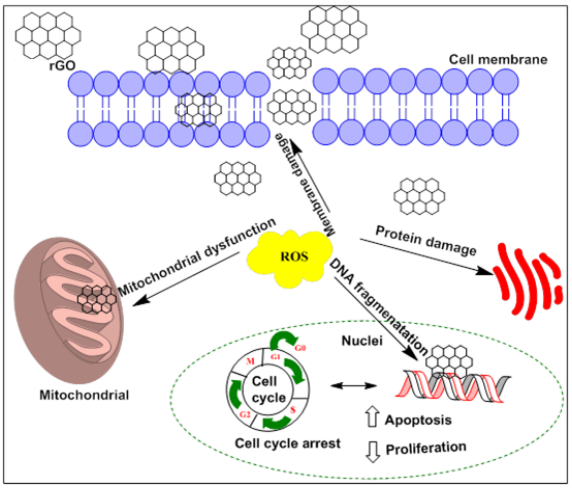

Figure 12. Anticancer activity proposed mechanism of reduced graphene oxide (rGO).

4. Conclusions

This study demonstrates a novel, eco-friendly route to synthesize reduced graphene oxide (rGO) using a methanolic extract of *Rhus coriaria* (L.) leaves (MERCL). The key finding of this work is the formation of a unique flower-plate nanostructure (MERCL-rGO), characterized by an ultra-thin, multi-layered morphology with an average size of approximately 9.6 nm. Comprehensive characterization confirmed the effective phytochemical-mediated reduction of GO, as evidenced by the restoration of the sp^2 carbon network and a significant increase in structural defect density (I_D/I_G = 1.08). The high abundance of essential oils, particularly oleic acid (31.76%), in MERCL is proposed as a critical factor driving the reduction process, suggesting a distinct mechanism compared to the polyphenol-dominated pathways commonly reported. The scientific contribution of this work is threefold: First, it establishes MERCL as an efficient reducing agent for the first time, highlighting the underexplored potential of essential oil-rich plant extracts in nanomaterial synthesis. Second, it yields a uniquely structured rGO nanomaterial with potential advantages for biomedical applications due to its high surface area and distinctive morphology. Third, it provides initial evidence of the dual cytotoxic and genotoxic effects of MERCL-rGO against MCF-7 breast cancer cells, with an IC_{50} of 212.8 µg/mL, linking its bioactivity to DNA damage induction. However, this study has several limitations that must be acknowledged. The research is confined to in vitro models, and the proposed reduction mechanism, while supported by

phytochemical data, requires further experimental validation, such as reactive oxygen species (ROS) generation and specific cell death pathways, to constrain a definitive mechanistic conclusion.

Author Contributions

Conceptualization, Z.S.A.A.; methodology, Z.S.A.A. and A.S.K.; formal analysis, A.S.K and Z.S.A.A.; investigation, A.S.K.; writing—original draft preparation, A.S.K.; writing—review and editing, Z.S.A.A.; visualization, A.S.K.; supervision, Z.S.A.A. All authors have read and agreed to the published version of the manuscript.

Institutional Review Board Statement

Not applicable.

Informed Consent Statement

Not applicable.

Data Availability Statement

Data supporting the findings of this study are available upon reasonable request from the corresponding author.

Funding

This research received no external funding.

Acknowledgments

Declared none.

Conflicts of Interest

The authors declare no conflict of interest.

References

1. Choi, W.; Lee, E.S. Therapeutic Targeting of DNA Damage Response in Cancer. *Int. J. Mol. Sci.* **2022**, *23*, 1701, https://doi.org/10.3390/ijms23031701.
2. Gyamfi, J.; Kim, J.; Choi, J. Cancer as a Metabolic Disorder. *Int. J. Mol. Sci.* **2022**, *23*, 1155, https://doi.org/10.3390/ijms23031155.
3. Arnold, M.; Morgan, E.; Rumgay, H.; Mafra, A.; Singh, D.; Laversanne, M.; Vignat, J.; Gralow, J.R.; Cardoso, F.; Siesling, S.; Soerjomataram, I. Current and future burden of breast cancer: Global statistics for 2020 and 2040. *Breast* **2022**, *66*, 15-23, https://doi.org/10.1016/j.breast.2022.08.010.
4. Ellsworth, R.E.; Blackburn, H.L.; Shriver, C.D.; Soon-Shiong, P.; Ellsworth, D.L. Molecular heterogeneity in breast cancer: State of the science and implications for patient care. *Semin. Cell Dev. Biol.* **2017**, *64*, 65-72, https://doi.org/10.1016/j.semcdb.2016.08.025.
5. Assi, H.A.; Khoury, K.E.; Dbouk, H.; Khalil, L.E.; Mouhieddine, T.H.; El Saghir, N.S. Epidemiology and prognosis of breast cancer in young women. *J. Thorac. Dis.* **2013**, *5*, S2–S8, https://doi.org/10.3978/j.issn.2072-1439.2013.05.24.
6. Giaquinto, A.N.; Sung, H.; Miller, K.D.; Kramer, J.L.; Newman, L.A.; Minihan, A.; Jemal, A.; Siegel, R.L. Breast cancer statistics, 2022. *CA Cancer J. clin.* **2022**, *72*, 524–541, https://doi.org/10.3322/caac.21754.

7. Talib, W.H.; AbuKhader, M.M. Combinatorial effects of thymoquinone on the anticancer activity and hepatotoxicity of the prodrug CB 1954. *Sci. Pharm.* **2013**, *81*, 519–530, https://doi.org/10.3797/scipharm.1211-15.
8. Zhai, J.; Wu, Y.; Ma, F.; Kaklamani, V.; Xu, B. Advances in medical treatment of breast cancer in 2022. *Cancer Innov.* **2023**, *2*, 1-17, https://doi.org/10.1002/cai2.46.
9. Choi, Y.-J.; Gurunathan, S.; Kim, J.-H. Graphene Oxide–Silver Nanocomposite Enhances Cytotoxic and Apoptotic Potential of Salinomycin in Human Ovarian Cancer Stem Cells (OvCSCs): A Novel Approach for Cancer Therapy. *Int. J. Mol. Sci.* **2018**, *19*, 710, https://doi.org/10.3390/ijms19030710.
10. Hossain, M.M.; Hamza, A.; Polash, S.A.; Tushar, M.H.; Takikawa, M.; Piash, A.B.; Dekiwadia, C.; Saha, T.; Takeoka, S.; Sarker, S.R. Green synthesis of silver nanoparticles using *Phyllanthus emblica* extract: investigation of antibacterial activity and biocompatibility *in vivo*. *RSC Pharm.* **2024**, *1*, 245-258, https://doi.org/10.1039/d3pm00077j.
11. Ibrahem, K.H. Green Synthesis of Nanoparticles Using Plants: A Comprehensive Review. *Kirkuk University J. Agri. Sci.***2025**, *16*, 72-78, https://doi.org/10.58928/ku25.16210.
12. Singh, J.; Jindal, N.; Kumar, V.; Singh, K. Role of green chemistry in synthesis and modification of graphene oxide and its application: A review study. *Chem. Phys. Impact* **2023**, *6*, 100185, https://doi.org/10.1016/j.chphi.2023.100185.
13. Keskin, C.; Aslan, S.; Baran, M.F.; Baran, A.; Eftekhari, A.; Adıcan, M.T.; Ahmadian, E.; Arslan, S.; Mohamed, A.J. Green synthesis and characterization of silver nanoparticles using *Anchusa officinalis*: antimicrobial and cytotoxic potential. *Int. J. Nanomedicine* **2025**, *20*, 4481-4502, https://doi.org/10.2147/IJN.S511217.
14. Al-Rikabi, J.M.; Al-Ali, Z.S.A.; Al-Naiema, I.M. The creation of a colorimetric aptasensor for ultrasensitive methamphetamine detection using gold nanoparticles. *Basrah J. Sci.* **2025**, *43*, 295-300.
15. Yi, J.; Choe, G.; Park, J.; Lee, J.Y. Graphene oxide-incorporated hydrogels for biomedical applications. *Polym. J.* **2020**, *52*, 823-837, https://doi.org/10.1038/s41428-020-0350-9.
16. Dash, B.S.; Jose, G.; Lu, Y.-J.; Chen, J.-P. Functionalized Reduced Graphene Oxide as a Versatile Tool for Cancer Therapy. *Int. J. Mol. Sci.* **2021**, *22*, 2989, https://doi.org/10.3390/ijms22062989.
17. Yang, J.; Xia, X.; He, K.; Zhang, M.; Qin, S.; Luo, M.; Wu, L. Green synthesis of reduced graphene oxide (RGO) using the plant extract of Salvia spinosa and evaluation of photothermal effect on pancreatic cancer cells. *J. Mol. Struct.* **2021**, *1245*, 131064, https://doi.org/10.1016/j.molstruc.2021.131064.
18. Manikandan, V.; Lee, N.Y. Reduced graphene oxide: Biofabrication and environmental applications. *Chemosphere* **2023**, *311*, 136934, https://doi.org/10.1016/j.chemosphere.2022.136934.
19. Mahmoud, A.E.D. Eco-friendly reduction of graphene oxide via agricultural byproducts or aquatic macrophytes. *Mater. Chem. Phys.* **2020**, *253*, 123336, https://doi.org/10.1016/j.matchemphys.2020.123336.
20. Li, B.; Jin, X.; Lin, J.; Chen, Z. Green reduction of graphene oxide by sugarcane bagasse extract and its application for the removal of cadmium in aqueous solution. *J. Clean. Prod.* **2018**, *189*, 128-134, https://doi.org/10.1016/j.jclepro.2018.04.018.
21. Kurmarayuni, C.M.; Kurapati, S.; Akhil, S.; Chandu, B.; Khandapu, B.M.K.; Koya, P.R.; Bollikolla, H.B. Synthesis of multifunctional graphene exhibiting excellent sonochemical dye removal activity, green and regioselective reduction of cinnamaldehyde. *Mater. Lett.* **2020**, *263*, 127224, https://doi.org/10.1016/j.matlet.2019.127224.
22. Haydari, I.; Aziz, K.; Kaya, S.; Daştan, T.; Ouazzani, N.; Mandi, L.; Aziz, F. Green synthesis of reduced graphene oxide and their use on column adsorption of phenol from olive mill wastewater. *Process Saf. Environ. Prot.* **2023**, *170*, 1079-1091, https://doi.org/10.1016/j.psep.2022.12.086.
23. Parvathi, E.; Akshaya, C.V.; Dilraj, N.; Arjun, G.; Deepak, N.K. Green synthesis of reduced graphene oxide by shallots. *Mater. Today Proc.* **2023**, https://doi.org/10.1016/j.matpr.2023.04.309.
24. Kadhim, A.S.; Al-Ali, Z.S.A. Green Synthesis of Reduced Graphene Oxide Nanosheets using Iraqi Rhus coriaria (L.) Fruits Extract and a Study of Its Anticancer Activity. *Iraqi J. Sci.* **2024**, *65*, 6253-6266, https://doi.org/10.24996/ijs.2024.65.11.5.
25. Kadim, A.S.; Al-Ali, Z.S.A. Reduce graphene oxide nanosheets derived from iraqi *Rhhus coriaria* (l.) fruits were evaluated for their anticancer and antibacterial properties. *Rev. Fac. Cienc.* **2024**, *13*, 49–72, https://doi.org/10.15446/rev.fac.cienc.v13n1.110790.
26. Bidan, A.K.; Al-Ali, Z.S.A. Oleic and Palmitic Acids with Bioderivatives Essential Oils Synthesized of Spherical Gold Nanoparticles and Its Anti-Human Breast Carcinoma MCF-7 *In Vitro* Examination. *BioNanoScience* **2023**, *13*, 2293-2306, https://doi.org/10.1007/s12668-023-01172-4.

27. Bidan, A.K.; Al-Ali, Z.S.A. Evaluation of cytotoxic potential of silver nanoparticles biosynthesized using essential oils of *Jasminum sambac* against breast cancer and bacterial cells. *3 Biotech* **2024**, *14*, 227, https://doi.org/10.1007/s13205-024-04058-8.
28. Bidan, A.K.; Al-Ali, Z.S.A. The role of biomaterial constituents of *Jasminum sambac* (L.) Aiton leaves in copper nanoparticles synthesis and evaluates their activities as anti-breast cancer and antibacterial agents. *Inorg. Nano-Met. Chem.* **2024**, *55*, 1-16, https://doi.org/10.1080/24701556.2024.2354480.
29. Budama-Kilinc, Y.; Arslan, E.; Gok, B.; Sari Yilmaz, M. Environmentally friendly green synthesis of reduced graphene oxide using *Laurus nobilis*, characterization and evaluation of *in vitro* anticancer activity. *Mater. Res. Express* **2025**, *12*, 015602, https://doi.org/10.1088/2053-1591/ada41d.
30. Zikalala, N.E.; Azizi, S.; Mpeta, L.S.; Ahmed, R.; Dube, A.; Mketo, N.; Zinatizadeh, A.A.; Mokrani, T.; Maaza, M.M. Green synthesis of reduced graphene oxide using *Persea americana* mill. extract: Characterization, oxygen reduction reaction and antibacterial application. *Diam. Relat. Mater.* **2024**, *149*, 111560, https://doi.org/10.1016/j.diamond.2024.111560.
31. Asgarpanah, J.; Saati, S. An overview on phytochemical and pharmacological properties of *Rhus coriaria* L. *Res. J. Pharmacogn.* **2014**, *1*, 47–54.
32. Mazaheri, T.; Hesarinejad, M.A.; Razavi, S.M.A.; Mohammadian, R.; Poorkian, S. Comparing physicochemical properties and antioxidant potential of sumac from Iran and Turkey. *MOJ Food Process. Technol.* **2017**, *5*, 288-294, https://doi.org/10.15406/mojfpt.2017.05.00125.
33. Marcano, D.C.; Kosynkin, D.V.; Berlin, J.M.; Sinitskii, A.; Sun, Z.; Slesarev, A.; Alemany, L.B.; Lu, W.; Tour, J.M. Improved Synthesis of Graphene Oxide. *ACS Nano* **2010**, *4*, 4806-4814, https://doi.org/10.1021/nn1006368.
34. Thiyagarajulu, N.; Arumugam, S.; Narayanan, A.L.; Mathivanan, T.; Renuka, R.R. Green Synthesis of Reduced Graphene Nanosheets using Leaf Extract of *Tridax procumbens* and its Potential *In Vitro* Biological Activities. *Biointerface Res. Appl. Chem.* **2020**, *11*, 9975-9984, https://doi.org/10.33263/BRIAC113.99759984.
35. Punniyakotti, P.; Aruliah, R.; Angaiah, S. Facile synthesis of reduced graphene oxide using *Acalypha indica* and *Raphanus sativus* extracts and their in vitro cytotoxicity activity against human breast (MCF-7) and lung (A549) cancer cell lines. *3 Biotech* **2021**, *11*, 157, https://doi.org/10.1007/s13205-021-02689-9.
36. Hinzmann, M.; Jaworski, S.; Kutwin, M.; Jagiełło, J.; Koziński, R.; Wierzbicki, M.; Grodzik, M.; Lipińska, L.; Sawosz, E.; Chwalibog, A. Nanoparticles containing allotropes of carbon have genotoxic effects on glioblastoma multiforme cells. *Int. J. Nanomedicine* **2014**, 2409-2417, https://doi.org/10.2147/IJN.S62497.
37. Senthil, R.A.; Selvi, A.; Arunachalam, P.; Amudha, L.S.; Madhavan, J.; Al-Mayouf, A.M. A sensitive electrochemical detection of hydroquinone using newly synthesized α-Fe_2O_3-graphene oxide nanocomposite as an electrode material. *J. Mater. Sci. Mater. Electron.* **2017**, *28*, 10081-10091, https://doi.org/10.1007/s10854-017-6769-x.
38. Aslam, M.; Kalyar, M.A.; Raza, Z.A. Synthesis and structural characterization of separate graphene oxide and reduced graphene oxide nanosheets. *Mater. Res. Express* **2016**, *3*, 105036, https://doi.org/10.1088/2053-1591/3/10/105036.
39. Perumal, D.; Albert, E.L.; Saad, N.; Hin, T.Y.Y.; Zawawi, R.M.; Teh, H.F.; Che Abdullah, C.A. Fabrication and Characterization of *Clinacanthus nutans* Mediated Reduced Graphene Oxide Using a Green Approach. *Crystals* **2022**, *12*, 1539, https://doi.org/10.3390/cryst12111539.
40. Mahata, S.; Sahu, A.; Shukla, P.; Rai, A.; Singh, M.; Rai, V.K. The novel and efficient reduction of graphene oxide using *Ocimum sanctum* L. leaf extract as an alternative renewable bio-resource. *New J. Chem.* **2018**, *42*, 19945-19952, https://doi.org/10.1039/C8NJ04086A.
41. Rochman, R.A.; Wahyuningsih, S.; Ramelan, A.H.; Hanif, Q.A. Preparation of nitrogen and sulphur Co-doped reduced graphene oxide (rGO-NS) using N and S heteroatom of thiourea. *IOP Conf. Ser.: Mater. Sci. Eng.* **2019**, *509*, 012119, https://doi.org/10.1088/1757-899X/509/1/012119.
42. Song, J.; Wang, X.; Chang, C.-T. Preparation and Characterization of Graphene Oxide. *J. Nanomater.* **2014**, *2014*, 276143, https://dx.doi.org/10.1155/2014/276143.
43. Toh, S.Y.; Loh, K.S.; Kamarudin, S.K.; Daud, W.R.W. Graphene production via electrochemical reduction of graphene oxide: Synthesis and characterisation. *Chem. Eng. J.* **2014**, *251*, 422-434, https://doi.org/10.1016/j.cej.2014.04.004.
44. Parthipan, P.; Al-Dosary, M.A.; Al-Ghamdi, A.A.; Subramania, A. Eco-friendly synthesis of reduced graphene oxide as sustainable photocatalyst for removal of hazardous organic dyes. *J. King Saud Univ. Sci.* **2021**, *33*, 101438, https://doi.org/10.1016/j.jksus.2021.101438.

45. Abdolhosseinzadeh, S.; Asgharzadeh, H.; Seop Kim, H. Fast and fully-scalable synthesis of reduced graphene oxide. *Sci. Rep.* **2015**, *5*, 10160, https://doi.org/10.1038/srep10160.
46. Zhu, X.; Xu, X.; Liu, F.; Jin, J.; Liu, L.; Zhi, Y.; Chen, Z.-w.; Zhou, Z.-s.; Yu, J. Green synthesis of graphene nanosheets and their in vitro cytotoxicity against human prostate cancer (DU 145) cell lines. *Nanomater. Nanotechnol.* **2017**, *7*, 1847980417702794, https://doi.org/10.1177/1847980417702794.
47. Tavakoli, F.; Salavati-Niasari, M.; badiei, A.; Mohandes, F. Green synthesis and characterization of graphene nanosheets. *Mater. Res. Bull.* **2015**, *63*, 51-57, https://dx.doi.org/10.1016/j.materresbull.2014.11.045.
48. Tambe, P. Synthesis and characterization of acid treated reduced graphene oxide. *Mater. Today Proc.* **2022**, *49*, 1294-1297, https://doi.org/10.1016/j.matpr.2021.06.381.
49. Qin, J.; Zhang, Y.; Lowe, S.E.; Jiang, L.; Ling, H.Y.; Shi, G.; Liu, P.; Zhang, S.; Zhong, Y.L.; Zhao, H. Room temperature production of graphene oxide with thermally labile oxygen functional groups for improved lithium ion battery fabrication and performance. *J. Mater. Chem. A* **2019**, *7*, 9646-9655, https://doi.org/10.1039/c9ta02244a.
50. Manchala, S.; Tandava, V.S.R.K.; Jampaiah, D.; Bhargava, S.K.; Shanker, V. Novel and Highly Efficient Strategy for the Green Synthesis of Soluble Graphene by Aqueous Polyphenol Extracts of Eucalyptus Bark and Its Applications in High-Performance Supercapacitors. *ACS Sustain. Chem. Eng.* **2019**, *7*, 11612-11620, https://doi.org/10.1021/acssuschemeng.9b01506.
51. Gao, X.; Tang, X. Effective reduction of graphene oxide thin films by a fluorinating agent: Diethylaminosulfur trifluoride. *Carbon* **2014**, *76*, 133-140, https://doi.org/10.1016/j.carbon.2014.04.059.
52. Saputra, A.M.A.; Marpongahtun; Andriayani; Goei, R.; Tok, A.I.Y.; Goutianos, S.; Gea, S. Facile synthesis of reduced graphene oxide using natural plant extracts as green reducing agents. *J. King Saud Univ. – Eng. Sci.* **2025**, *37*, 5, https://doi.org/10.1007/s44444-025-00007-9.
53. Pareek, S.; Jain, D.; Shrivastava, R.; Dam, S.; Hussain, S.; Behera, D. Tunable degree of oxidation in graphene oxide: cost effective synthesis, characterization and process optimization. *Mater. Res. Express***2019**, *6*, 085625, https://doi.org/10.1088/2053-1591/ab243a.
54. Johra, F.T.; Lee, J.-W.; Jung, W.-G. Facile and safe graphene preparation on solution based platform. *J. Ind. Eng. Chem.* **2014**, *20*, 2883-2887, https://doi.org/10.1016/j.jiec.2013.11.022.
55. Bo, Z.; Shuai, X.; Mao, S.; Yang, H.; Qian, J.; Chen, J.; Yan, J.; Cen, K. Green preparation of reduced graphene oxide for sensing and energy storage applications. *Sci. Rep.* **2014**, *4*, 4684, https://doi.org/10.1038/srep04684.
56. Li, C.; Zhuang, Z.; Jin, X.; Chen, Z. A facile and green preparation of reduced graphene oxide using *Eucalyptus* leaf extract. *Appl. Surf. Sci.* **2017**, *422*, 469-474, https://doi.org/10.1016/j.apsusc.2017.06.032.
57. Azizighannad, S.; Mitra, S. Stepwise Reduction of Graphene Oxide (GO) and Its Effects on Chemical and Colloidal Properties. *Sci. Rep.* **2018**, *8*, 10083, https://doi.org/10.1038/s41598-018-28353-6.
58. Kadiyala, N.K.; Mandal, B.K.; Ranjan, S.; Dasgupta, N. Bioinspired gold nanoparticles decorated reduced graphene oxide nanocomposite using *Syzygium cumini* seed extract: Evaluation of its biological applications. *Mater. Sci. Eng., C* **2018**, *93*, 191-205, https://doi.org/10.1016/j.msec.2018.07.075.
59. Ghosh, S.; Das, P.; Baskey, M. Plant extract assisted synthesis of reduced graphene oxide sheet and the photocatalytic performances on cationic and anionic dyes to decontaminate wastewater. *Adv. Nat. Sci: Nanosci. Nanotechnol.* **2021**, *12*, 015008, https://doi.org/10.1088/2043-6254/abde41.
60. Chatterjee, N.; Eom, H.-J.; Choi, J. A systems toxicology approach to the surface functionality control of graphene–cell interactions. *Biomaterials* **2014**, *35*, 1109-1127, https://doi.org/10.1016/j.biomaterials.2013.09.108.
61. Zhang, J.; Cao, H.-Y.; Wang, J.-Q.; Wu, G.-D.; Wang, L. Graphene Oxide and Reduced Graphene Oxide Exhibit Cardiotoxicity Through the Regulation of Lipid Peroxidation, Oxidative Stress, and Mitochondrial Dysfunction. *Front. Cell Dev. Biol.* **2021**, *9*, 616888, https://doi.org/10.3389/fcell.2021.616888.
62. Abu-Reidah, I.M.; Ali-Shtayeh, M.S.; Jamous, R.M.; Arráez-Román, D.; Segura-Carretero, A. HPLC–DAD–ESI-MS/MS screening of bioactive components from *Rhus coriaria* L. (Sumac) fruits. *Food Chem.* **2015**, *166*, 179-191, https://doi.org/10.1016/j.foodchem.2014.06.011.
63. Kubatka, P.; Kello, M.; Kajo, K.; Samec, M.; Liskova, A.; Jasek, K.; Koklesova, L.; Kuruc, T.; Adamkov, M.; Smejkal, K.; Svajdlenka, E.; Solar, P.; Pec, M.; Büsselberg, D.; Sadlonova, V.; Mojzis, J. *Rhus coriaria* L. (Sumac) Demonstrates Oncostatic Activity in the Therapeutic and Preventive Model of Breast Carcinoma. *Int. J. Mol. Sci.* **2021**, *22*, 183, https://doi.org/10.3390/ijms22010183.

64. Wu, K.; Zhou, Q.; Ouyang, S. Direct and Indirect Genotoxicity of Graphene Family Nanomaterials on DNA—A Review. *Nanomaterials* **2021**, *11*, 2889, https://doi.org/10.3390/nano11112889.
65. Krętowski, R.; Cechowska-Pasko, M. The Reduced Graphene Oxide (rGO) Induces Apoptosis, Autophagy and Cell Cycle Arrest in Breast Cancer Cells. *Int. J. Mol. Sci.* **2022**, *23*, 9285, https://doi.org/10.3390/ijms23169285.
66. Gul, W.; Akbar Shah, S.R.; Khan, A.; Ahmad, N.; Ahmed, S.; Ain, N.; Mehmood, A.; Salah, B.; Ullah, S.S.; Khan, R. Synthesis of graphene oxide (GO) and reduced graphene oxide (rGO) and their application as nano-fillers to improve the physical and mechanical properties of medium density fiberboard. *Front. Mater.* **2023**, *10*, 1206918, https://doi.org/10.3389/fmats.2023.1206918.

Publisher's Note & Disclaimer